Available online at www.sciencedirect.com
SCIENCE DIRECT®
Journal of Sound and Vibration 277 (2004) 855–879
JOURNAL OF SOUND AND VIBRATION
www.elsevier.com/locate/jsvi

Studies on linear thermoelastic buckling and free vibration analysis of geometrically perfect hemispherical shells with cut-out

N. Ganesan*, Ravikiran Kadoli

Machine Dynamics Laboratory, Department of Applied Mechanics, Indian Institute of Technology Madras, Chennai 600 036, India

Received 20 March 2003; accepted 15 September 2003

Abstract

Thermoelastic buckling and free vibration analysis of geometrically perfect isotropic hemispherical shells subjected to axisymmetric temperature variation are presented. First order shear deformation theory is used to analyze the moderately thick elastic hemispherical shells. The variations of various field variables are assumed in the circumferential direction and the finite element matrices used in the numerical studies are based on the semi-analytical method. The formulation is validated for thermal buckling strains available in the literature. Thermal buckling temperatures are evaluated for deep shells having a cut-out at the apex. Parameters considered in the study include hemispherical shells with a/h ratios of 100 and 500 and each with cut-out angle at apex equal to 7°, 30° and 45°. Boundary conditions considered are clamped–clamped and clamped–free. A study on the distribution of the stress resultants due to thermal loading is examined in order to relate their influence on the buckling temperature of the shells with respect to above-stated geometric parameters. The effect of temperature on the free vibration natural frequency of the hemispherical shell is also analyzed.

1. Introduction

Spherical shells prominently find great use for containing fluid under normal as well as high pressure, especially in the oil and chemical industries. Most commonly, part of the full sphere mainly in the form of hemisphere or shallow sphere forms a primary part of the whole assembly as in the fuel tank, propellant tank, combustion chambers, submarines, satellites, to quote few

*Corresponding author. Tel.: +91-44-2351365; fax: +91-44-2350509.
E-mail address: nganesan@iitm.ac.in (N. Ganesan).

0022-460X/$ - see front matter © 2003 Elsevier Ltd. All rights reserved.
doi:10.1016/j.jsv.2003.09.008

examples. Spherical shells are used as containment vessel for nuclear reactor in nuclear power plant. It is well known that components taking the form of a sphere or part of the sphere are capable of withstanding high-pressure loads. But the practical limitation is the high cost involved in the manufacture of spherical components.

A detailed review of the literature which encompasses stability studies on perfect and imperfect shallow spherical shells under pressure loading using non-linear theories is presented. Few review articles on vibration of shells, thermal buckling of plates and shells, and computational models used for studies of plates and shells under high temperature are also presented. Buckling phenomenon in shells either due to mechanical compressive pressure loading as well as compressive loading at sufficient elevated temperature is highly complex in nature. It is well understood that buckling of shells is highly sensitive to geometric imperfection which are inherent during the fabrication processes. Inconsistency of sphericity, thickness and presence of residual stresses are few parameters that can be present in an imperfect shell. The theoretical prediction of the buckling load grossly overestimates the actual buckling load when determined from experiments. Teng [1] has laid great emphasis on the aspects that govern the buckling load of thin shells in his review article. Teng reviews the works on buckling of thin shells which have considered geometric imperfection, uniform loading, wind and earthquake loads, non-uniform torsion, localized circumferential compression, local axial compression and non-uniform external pressure. He also points the role and contribution of the research community in making the numerical shell buckling analysis in design to be directly used in predicting the buckling strength. Thornton [2] has presented a detailed review on the thermal buckling and post-buckling of plates, cylindrical panels, shallow shells, cylindrical shells and conical shells. It is stated that the magnitude of temperature, its variation and distribution has enormous consequence on the thermal buckling behavior. Thermal buckling analysis is highly complex in aerospace structures and orbiting space structures mainly due to non-uniform temperature exposure as well as radiation heat transfer and also due to presence of adjoining components. The review article concludes that advanced composite materials are suitable candidates for achieving better performance under the action of the combined loading. In the review article which deals on dynamic behavior of homogeneous shells by Qatu [3], it can be seen that in the last one decade there are few reported research articles on the aspects considering the thermal effects on dynamic behavior of cylindrical, conical and shallow spherical shells. Noda [4] reviews the nature of the articles published on thermal stresses in structural components and components involved in the manufacturing processes like casting and welding which considers the material properties dependent on temperature. Noor and Burton [5] makes an exhaustive review in the computational area of multilayered composite plates and shells subjected to high temperature. Brief discussion on the advantages and disadvantages of various shell theories used for the study of vibration behavior of shells has been dealt in the review article of Liew et al. [6].

Archer [7] investigated the influence of uniform tensile and compressive stress states on the natural frequencies of shallow spherical shells using the shallow shell equations containing the inertial loading term. Fitch [8] used Marguerre's non-linear shallow shell theory to carry out investigation on the axisymmetric as well as asymmetric buckling behavior for a clamped shallow spherical cap. Pedersen and Jensen [9] outlines a detailed analytical procedure for the practical design in determining the buckling load of spherical shells highly sensitive to geometrical imperfections subjected to complicated static and dynamic loads. They illustrated the design

procedure for cargo tanks in ship used for transportation of liquefied natural gas and large spherical containment shells for nuclear power plant. Studies conducted by Yao [10] on truncated hemispherical shells under axial tension led to the conclusion that when the axial tensile load reaches a critical value the hoop stress causes the truncated hemisphere to buckle. Krenzke and Kiernan [11] compared the experimental results of the collapse pressure (buckling pressure) for a near perfect shallow spherical shells with the results from the theory of symmetric buckling developed by Budiansky, Weinitschke and Thruston (in case of short clamped spherical shell segments) and non-symmetric buckling theory developed by Huang (in case of longer clamped spherical shell segments). Huang [12] derived the governing equations for the study of unsymmetrical buckling of clamped shallow shells subjected to uniform pressure and undergoing unsymmetrical deformation just below the critical buckling pressure (for the case of axisymmetrical deformation). Fitch and Budiansky [13] presented an analysis for the buckling and post-buckling behavior of a clamped spherical cap uniformly loaded over a circular region centered at the apex. They report the findings on the effect of increasing the area of the loading region on the buckling and post-buckling behavior. Gu [14] worked on the buckling behavior of clamped shallow spherical shells with a center hole, and in particular examined the effects of the hole with different radii and two kinds of boundary conditions on the buckling behavior. Gonçalves [15] used the fourth order Maguerre's shallow shell equations to carry out studies on the influence of axisymmetric initial geometric imperfections and a non-linear compressive stress state on the natural frequencies of the clamped shallow spherical shells.

Williams [16] considered the equations governing the stresses and displacements in a spherical shell due to axisymmetric temperature distribution given by Boley and Weiner. He presented the thermoelasticity solutions to the equations of thin spherical shells by the method of matched asymptotic expansion which also incorporates the order of magnitude analysis. Formulae for computing meridional and circumferential stress components are presented for sufficiently thin spherical shells. Krizhevsky and Stavsky [17] carried out investigation on the sensitivity of axisymmetric buckling loads for orthotropic shallow spherical shells subjected to steady state thermal field. Aggarwala [18] conducted studies on the thermal instability of simply supported bimetallic shallow spherical shells. Liu [19] has developed a non-linear thermal stability theory for the analysis of bimetallic shallow spherical shells and truncated conical shells subjected to uniform temperature field, which are important component of many precision instruments. Jayaraman and Rao [20] computed the stress variations in a spherical shell with a conical nozzle under conditions of uniform heating as well as uniform heating but temperature varying linearly across the thickness. Jianping and Harik [21] presented an iterative finite difference procedure for the analysis of spherical shells with varying wall thickness and subjected to pressure and surface temperature loading. Variation of material properties with respect to temperature were used according to AISC: Specification 1988. The inner and outer surface tangential stresses were computed and were in good agreement with results obtained using ANSYS. Kapania and Mohan [22] developed a flat triangular shell element using the Discrete Kirchhoff Theory plate bending element and Linear Strain Triangular membrane element. This element was used to carry out free vibration and thermal analysis of laminated plates and spherical shells under different loading conditions.

Few among the notable research studies on the thermal buckling of thin walled cylindrical shells are due to Hoff [23], Abir and Nardo [24], Zuk [25] and Radhamohan and Venkataramana [26].

Instability of truncated conical shells under thermal loading was studied by Lu and Chang [27]. The recent work on thermal buckling of spherical shells is reported by Eslami et al. [28], Sanders and Donnel–Musthari–Vlasov non-linear strain–displacement relations are utilized to determine the thermal buckling load for uniform temperature loading and radial temperature difference loading cases.

Thus it is clear that there exist very few research articles reported on linear thermoelastic buckling of hemispherical shells with cut-out as well as studies on the effect of uniform temperature on the free vibration natural frequency. This work presents the numerical results on the thermal buckling temperature for hemispherical shells with a cut-out at the apex for two edge conditions. Meridional stress resultants and hoop stress resultants are computed to correlate the magnitude of buckling temperature. The effects of the magnitude of the angle of cut-out at apex as well as the boundary conditions at the edge are studied. Few numerical results are also presented to illustrate the effect of temperature on the free vibratory natural frequency of the hemispherical shells. The numerical computation is based on the strain–displacement relations for general shells of revolution which accounts for transverse shear deformation. Using the semi-analytical method the finite element stiffness and mass matrix of the shell are computed. A uniform temperature distribution is assumed to exist over the shell and temperature across the wall thickness is constant. Assuming the various material properties to be independent of temperature, thermal loading under isothermal conditions is computed. The geometric stiffness matrix thus results from the initial stress resultants and moment resultants. This makes possible for a simple thermoelastic buckling analysis and free vibration analysis of initially stressed hemispherical shells with cut-out at apex due to uniform temperature rise.

2. Semi-analytical finite element method for analysis of hemispherical shells with cut-out at apex

The following assumptions are considered in the formulation and subsequent analysis: The hemispherical shell is geometrically perfect, homogeneous and isotropic. In determining critical buckling temperature small bending displacements of the shell are assumed, material properties are independent of temperature, temperature through the thickness of shell is uniform and overall the shell is subjected to a constant thermal loading. In effect we use an uncoupled formulation for the thermoelastic buckling and free vibration analysis.

2.1. Structural stiffness and mass matrix

The details of the formulation are same as that presented in the recent article published by the authors on the study of buckling and dynamic analysis of composite cylindrical shell bonded with PZT layers, Ganesan and Kadoli [29]. The present study uses the same formulation for the reason that the semi-analytical finite element for the shell laminate developed by Rao and Ganesan [30] is for a general shells of revolution. Hence one needs to define the proper geometric variables like the quantities R_ϕ and R_θ.

Accordingly from Fig. 1, the quantities $R_\phi(O_2Q)$ and $R_\theta(O_3Q)$, the principle radii of curvature of the shell are set equal to same magnitude and thereby the co-ordinate details for hemispherical shell can be obtained.

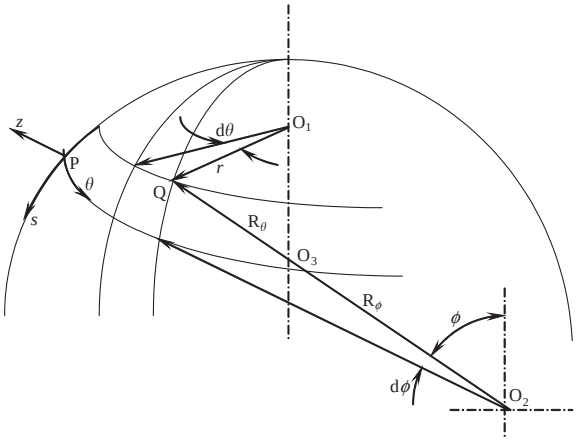

Fig. 1. Orthogonal curvilinear co-ordinate system for doubly curved shells.

The evaluation of thermal load vector and the resulting initial stress resultants and moment resultants are based on first order shear deformation theory (FSDT). The stiffness matrix and the geometric stiffness matrix are evaluated by considering the total strain energy in shell

$$U = U_1 + U_2,$$

where U_1 is the strain energy due to vibratory stresses and U_2 is the strain energy due to initial stresses which results from steady state temperature. Strain energy U_1 is given by

$$U_1 = \frac{1}{2}\int_V \left\{\varepsilon_{ss}\sigma_{ss} + \varepsilon_{\theta\theta}\sigma_{\theta\theta} + \gamma_{\theta z}\tau_{\theta z} + \gamma_{sz}\tau_{sz} + \gamma_{s\theta}\tau_{s\theta}\right\} \mathrm{d}V.$$

The kinematic relations for a doubly curved shells of revolution in the (s, θ, z) co-ordinate based on FSDT are as follows, see Rao and Ganesan [30]:

$$\varepsilon_{ss} = (\varepsilon^0_{ss} + z\kappa^1_s)/A_1, \quad \gamma_{\theta z} = \gamma^0_{\theta z}/A_2,$$

$$\varepsilon_{\theta\theta} = (\varepsilon^0_{\theta\theta} + z\kappa^1_\theta)/A_2, \quad \gamma_{sz} = \gamma^0_{sz}/A_1,$$

$$\gamma_{s\theta} = \frac{1}{A_1}\frac{1}{A_2} \quad (\gamma^0_{s\theta} + z\kappa^1_{s\theta}),$$

where

$$\frac{1}{A_1} = \frac{1}{(1 + z/R_\phi)} \quad \text{and} \quad \frac{1}{A_2} = \frac{1}{(1 + z/R_\theta)}$$

in the above equations R_ϕ and R_θ are the principle radii of curvature of the shell and z is the thickness measured along the z-axis. In the above equation, $\varepsilon_{ss}, \varepsilon_{\theta\theta}, \gamma_{\theta z}, \gamma_{sz}, \gamma_{s\theta}$ are the total strains which comprise of the normal strains and the shear strains, $\varepsilon^0_{ss}, \varepsilon^0_{\theta\theta}, \gamma^0_{\theta z}, \gamma^0_{sz}, \gamma^0_{s\theta}$, referred to mid-surface and $\kappa^1_s, \kappa^1_\theta, \kappa^1_{s\theta}$, the change in curvature of the mid-surface. The mid-surface strains and

strains due to change of curvature for a general shell of revolution are described as follows:

$$\varepsilon_{ss}^0 = \frac{\partial u_0}{\partial s} + \frac{w}{R_\phi}, \quad \varepsilon_{\theta\theta}^0 = \frac{1}{r}\frac{\partial v_0}{\partial \theta} + \frac{u_0}{r}\cos\phi + \frac{w_0}{r}\sin\phi,$$

$$\gamma_{\theta z}^0 = \phi_\theta - \frac{v_0}{r}\sin\phi + \frac{1}{r}\frac{\partial w_0}{\partial \theta}, \quad \gamma_{s\theta}^0 = \frac{1}{r}\frac{\partial u_0}{\partial \theta} + \frac{\partial v_0}{\partial s} - \frac{v_0}{r}\cos\phi$$

$$\gamma_{sz}^0 = \phi_s - \frac{u_0}{R_\phi} + \frac{\partial w_0}{\partial s},$$

$$\kappa_s^1 = \frac{\partial \phi_s}{\partial s}, \quad \kappa_\theta^1 = \frac{1}{r}\frac{\partial \phi_\theta}{\partial \theta} + \frac{\phi_s}{r}\cos\phi,$$

$$\kappa_{s\theta}^1 = \frac{1}{r}\frac{\partial \phi_s}{\partial \theta} + \frac{\partial \phi_\theta}{\partial s} - \frac{\phi_\theta}{r}\cos\phi + \frac{\sin\phi}{r}\frac{\partial v_0}{\partial s} + \frac{1}{R_\phi r}\frac{\partial u_0}{\partial \theta} - \frac{v_0}{R_\phi r}\cos\phi.$$

In the above equations r represents the parallel-circle radius to the shell mid-surface, and can be inferred from Fig. 1 as $r = R_\theta \sin\phi$. The elastic constant matrix comprising various integrated shell stiffnesses (A_{ij}, B_{ij}, D_{ij} and F_{ij}) relates the stress and moment resultants vector, $\{\mathbf{N}\}$, and strain vector, $\{\boldsymbol{\varepsilon}\}$.

$$\{\boldsymbol{\varepsilon}\}^{\mathrm{T}} = \{\varepsilon_{ss}^0 \;\; \varepsilon_{\theta\theta}^0 \;\; \gamma_{s\theta}^0 \;\; \kappa_s^1 \;\; \kappa_\theta^1 \;\; \kappa_{s\theta}^1 \;\; \gamma_{sz}^0 \;\; \gamma_{\theta z}^0\},$$

$$\{\mathbf{N}\}^{\mathrm{T}} = \{N_{ss} \;\; N_{\theta\theta} \;\; N_{s\theta} \;\; M_{ss} \;\; M_{\theta\theta} \;\; M_{s\theta} \;\; Q_s \;\; Q_\theta\},$$

$$(A_{ij}, B_{ij}, D_{ij}, F_{ij}) = \int_{-h/2}^{+h/2} \bar{Q}_{ij}(1, z, z^2, z^3)\,\mathrm{d}z.$$

The methodology for the derivation of the element stiffness matrix for the shell laminate is based on the usual finite element procedure. Shear correction factor equal to $\frac{5}{6}$ is used. The mass matrix is obtained from the kinetic energy of the shell continuum,

$$KE = \frac{\rho}{2}\int_V (\dot{u}^2 + \dot{v}^2 + \dot{w}^2)\,\mathrm{d}V.$$

The strain energy due to initial stresses U_2, which is stated in Rao [31], is used to evaluate the geometric stiffness matrix. Neglecting the strain energy due to transverse shear stresses, the expression for the strain energy due to initial stresses U_2 is

$$U_2 = \frac{1}{2}\int_V \{(\varepsilon_{ss}^i)^2\sigma_{ss}^* + (\varepsilon_{\theta\theta}^i)^2\sigma_{\theta\theta}^* + 2\gamma_{s\theta}^i\tau_{s\theta}^*\}\,\mathrm{d}V,$$

where σ_{ss}^*, $\sigma_{\theta\theta}^*$ and $\tau_{s\theta}^*$ are the initial stresses and the corresponding non-linear strains ε_{ss}^i, $\varepsilon_{\theta\theta}^i$ and $\gamma_{s\theta}^i$ are given as follows:

$$\varepsilon_{ss}^i = \frac{1}{(1 + z/R_\phi)}\left(\frac{\partial w^i}{\partial s} - \frac{u^i}{R_\phi}\right),$$

$$\varepsilon_{\theta\theta}^i = \frac{1}{(1 + z/R_\theta)}\left(\frac{1}{r}\frac{\partial w^i}{\partial \theta} - \frac{v^i}{r}\sin\phi\right),$$

$$\gamma_{s\theta}^i = \varepsilon_{ss}^i\varepsilon_{\theta\theta}^i.$$

In the semi-analytical approach, the generalized displacement field is assumed to depend in the circumferential direction for various harmonics as follows:

$$u_0 = \sum_{m=0}^{\infty} u_{0m} \cos m\theta, \quad v_0 = \sum_{m=0}^{\infty} v_{0m} \sin m\theta, \quad w_0 = \sum_{m=0}^{\infty} w_{0m} \cos m\theta,$$

$$\psi_{0s} = \sum_{m=0}^{\infty} \psi_{0sm} \cos m\theta, \quad \psi_{0\theta} = \sum_{m=3}^{\infty} \psi_{0\theta m} \sin m\theta,$$

where u_0, v_0 and w_0 represents the mid-surface displacements. ψ_{0s} and $\psi_{0\theta}$ are the shear rotations of the mid-surface normal. 'm' represents the circumferential mode number. Various Fourier harmonics would be decoupled if one considers only small vibrations.

2.2. Thermal load and initial stress evaluation

The study considers a situation where the hemispherical shell is maintained at a constant temperature so that temperature is constant over the thickness of the shell, $T(s, \theta, z, t) = T(s, \theta, t)$. In semi-analytical approach we assume the temperature to vary in the θ direction. Based on Fourier series expansion, the temperature will be expressed as

$$T = \sum_{m=0}^{\infty} T_m \cos m\theta.$$

When a body is maintained at a temperature above the stress-free (or reference) temperature, this will result in the initial strains in the body. The potential for a continuum under thermal environment is given by

$$\Pi = \frac{1}{2} \int_V \{\boldsymbol{\varepsilon}\}^{\mathrm{T}} [\mathbf{D}] \{\boldsymbol{\varepsilon}\} \, \mathrm{d}V - \int_V \{\boldsymbol{\varepsilon}\}^{\mathrm{T}} \{\boldsymbol{\lambda}\} T \, \mathrm{d}V,$$

where $\{\boldsymbol{\varepsilon}\}$ is the strain vector, $\{\boldsymbol{\lambda}\}$ is the vector of temperature stress coefficients and T is the temperature rise from the stress free temperature. Based on the minimization of the total potential, in the above equation the second term will yield the thermal load vector. One can compute the thermal load vector and thereby determine displacement field due to thermal load. Finally, the stress resultants and moment resultants are obtained which will be used to compute the geometric stiffness matrix. The interested readers can refer to Ref. [29] for the detailed procedure.

3. Numerical results and analysis

The numerical study mainly comprises of the computation of the lowest thermal buckling temperature for different circumferential modes and to study the effect of temperature on the natural frequency of the hemispherical shells. The classical buckling eigenvalue problem is formulated comprising the global stiffness matrix and the global geometric stiffness matrix of the hemispherical shell to obtain the buckling eigenparameters for an arbitrary temperature rise. Hemispherical shells with $a/h = 100$ and 500 each having a cut-out at the apex are analyzed. The size of the cut-out at the apex is specified indirectly by stating the angle subtended by the cut-out

with the center of the hemisphere. Hence cut-out angle equal to 7°, 30° and 45° are considered for the study and the geometry of each hemisphere is illustrated in Fig. 2. The base radius 'a' of the hemispherical shell is equal to 1.0 m and 'h' denotes the thickness of the shell. The edge conditions are clamped–clamped at the open circular edges, and clamped–free, i.e. clamped at the larger circular edge and the edge at the cut-out portion at the apex is free, see Fig. 2(b) and (c). The hemispherical shells will be referred with the following names as mentioned in Table 1 for the subsequent discussion.

The distribution of the total stress resultants and moment resultants along the meridian of the hemisphere are also presented in order to explain the dependence of thermal buckling temperature on the stress and moment resultants. Based on the convergence study the number of finite elements is decided for the analysis. The finite element code used for the computation of the buckling temperature is validated against the results as reported in the literature.

Subsequently, a detailed discussion is presented on the numerical results on the thermal buckling temperature of hemispherical shell with cut-out at the apex. Free vibration natural frequencies are computed at temperatures other than stress free temperature in order to study the effect of temperature. Results presented are restricted to hemispherical shell with $a/h = 500$ and clamped–clamped boundary condition.

3.1. Convergence study

A typical hemispherical shell with $a/h = 100$, $S/a = 1.0$, base radius equal to 1.0 m, with dome height S and cut out at apex equal to 7° is considered. Three finite element models with number of elements equal to 30, 40 and 50 are considered in the initial study. Fig. 3 shows the typical finite element mesh of the hemispherical shell using a three-node quadratic line element. The finite

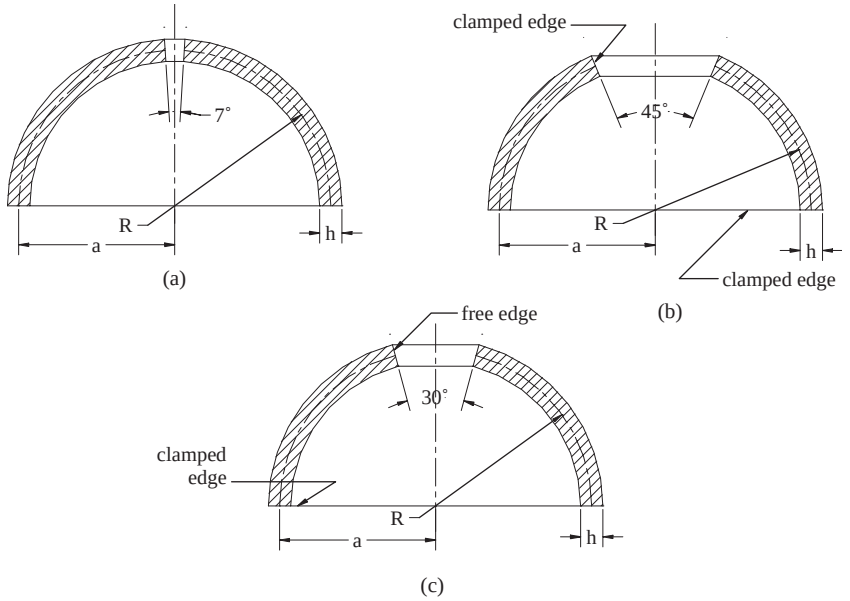

Fig. 2. Illustration of the geometry of hemispherical shells and boundary conditions.

Table 1
Nomenclature of the hemispherical shells referred in text

Cut-out angle (deg)	a/h	
	100	500
7	Shell A1	Shell A2
30	Shell B1	Shell B2
45	Shell C1	Shell C2

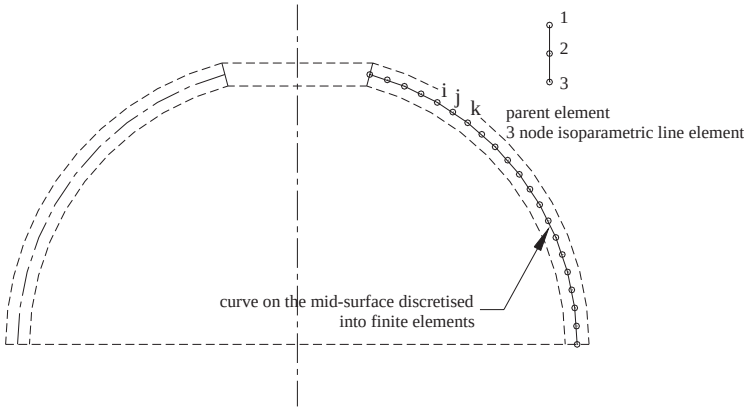

Fig. 3. Typical illustration of the finite element mesh of the hemispherical shell with cut-out at apex using a three-node quadratic line element.

element mesh is created in the s-co-ordinate along the mid-surface of the shell. The hemispherical shell was clamped at both circular edges, illustrated in Fig. 2(b). Using these finite element models the lowest buckling temperature associated with first 30 circumferential modes were computed.

Since one is interested in the lowest buckling temperature from the design point of view, Table 2 lists the lowest buckling temperature T_{cri} and its associated mode (m, n), where m represents the circumferential harmonic and n stands for the axial mode number.

There is monotonic convergence for the lowest buckling temperature. Based on the above observation and from the point of view of lesser computational time, it is reasonable to use 30 elements for the finite element analysis.

3.2. Validation of the formulation

The semi-analytical finite element formulation for the computation of thermal buckling temperature is validated against the work of Eslami et al. [28]. Fig. 4 illustrates the typical configuration of the hemispherical shell considered for the study.

The spherical shell is simply supported at the edges, such that $w_1 = w_{1,\phi\phi} = v_1 = u_{1,\phi} = 0$ was assumed. Symmetric boundary condition at the apex of the shell considered is as follows: $v_0 = w_0 = \psi_{0\theta} = 0$ (i.e. restrained) and u_0, ψ_{0s} motion and rotation are permitted. The analysis is based

Table 2
Convergence of the lowest buckling temperature

Sl. No.	Number of elements	Lowest buckling temperature T_{cri}°C	Mode (m,n)
1.	30	3627.3	(25,1)
2.	40	3559.6	(25,1)
3.	50	3535.1	(25,1)

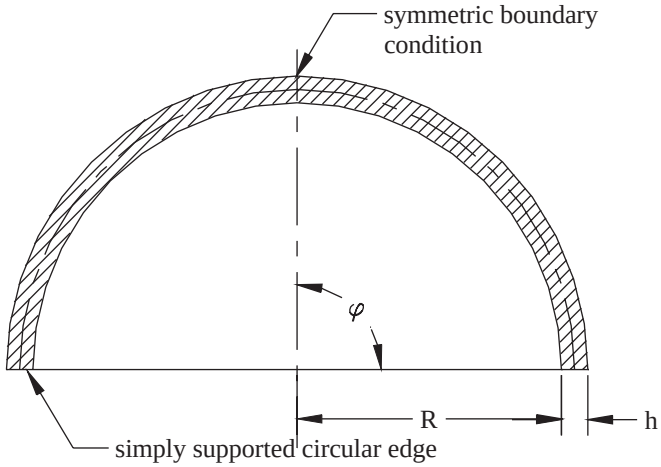

Fig. 4. Hemispherical shell with simply supported circular edge and symmetric boundary condition at the apex.

on symmetric distribution of thermal buckling load. The prebuckling forces $N_{\phi 0}$ and $N_{\theta 0}$ will dictate the equilibrium of the shell. Using the present formulation computation of thermal buckling strains for hemispherical shell with latitude angle, $\varphi = \pi/2$, and for various ratios of h/R (0.01, 0.02, 0.03, 0.04, 0.05, 0.06, 0.07, 0.08, 0.09 and 0.10) is carried out using the prebuckling forces as described in Eslami et al. Comparisons of the thermal buckling strain and their associated modes are presented in Table 3. The material used is an isotropic with $\upsilon = 0.3$.

Table 3 compares the lowest thermal buckling strain and the associated mode obtained by thin shell theory (Eslami et al.) and general shell theory for moderately thick shells (present). The percentage difference between the result increases with increase in h/R. This is expected since the present computation is based on the thick shell theory. Further it should be noticed that the buckling strains obtained from the two theory holds well for $h/R = 0.01$–0.05. Hence it is reasonable to use the present formulation for a detailed study on the thermal-buckling behavior and free vibration characteristics of the hemispherical shell under axisymmetric temperature.

3.3. Thermal buckling temperature for hemispherical shell with cut-outs and clamped–clamped boundary condition

Hemispherical shells with $a/h = 100$ and 500, base radius equal to 1.0 m and the thickness of the shell equal to 10.0 and 2.0 mm are considered for the study. Each shell will have a cut-out at

Table 3
Validation of thermal buckling strains evaluated using deep shell theory and FSDT considering the prebuckling forces

h/R	Deep shell theory Eslami et al. [28]	Present FSDT	Percentage difference (%)
0.01	0.004130(9,1)	0.004071(9,1)	1.4
0.02	0.008435(6,1)	0.008435(5,1)	3.9
0.03	0.011200(5,1)	0.01204(5,1)	0.3
0.04	0.017260(5,1)	0.01624(5,1)	5.9
0.05	0.021490(4,1)	0.02034(4,1)	5.1
0.06	0.026140(4,1)	0.023786(4,1)	9.1
0.07	0.031620(4,1)	0.027644(4,1)	12.6
0.08	0.035740(1,1)	0.031643(1,1)	11.48
0.09	0.039910(1,1)	0.03530(1,1)	11.5
0.10	0.044570(1,1)	0.039272(1,1)	11.9

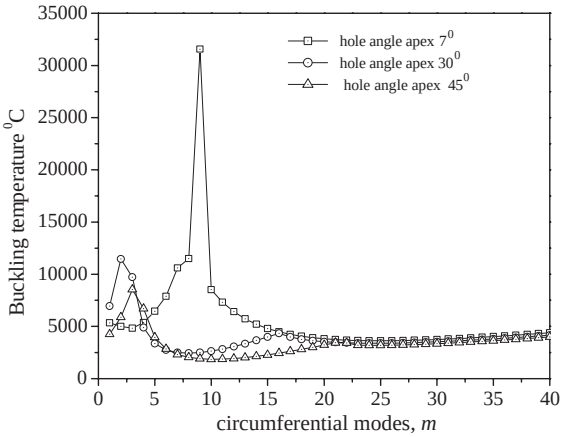

Fig. 5. Lowest buckling temperature for a clamped–clamped hemispherical shells with $a/h = 100$.

the apex which subtends an angle 7°, 30° and 45° with the center of the shell. These details are clear from Fig. 2.

The magnitude of the buckling temperature presented in the study are absolute values, $T_{abs.}$. The buckling temperatures are obtained for an arbitrary temperature rise of 30°C. These temperatures correspond to ΔT, where $\Delta T = T_{abs} - T_0$, where T_0 corresponds to the stress-free temperature assumed equal to 20°C. Fig. 5 provides a graphical picture of the magnitude of the lowest thermal buckling temperatures associated with first 40 circumferential modes for shell with $a/h = 100$. In general, it is found that the buckling temperatures are excessively high and it is highly impractical to think of operating mild steel at such temperatures or in other words any mild steel components are never put into long operation beyond temperatures of 200–300°C. It is seen that the buckling temperatures for hemispherical shell A1 initially increases with increase in number of modes, reaches a peak and then reduces as the circumferential mode number increases.

The lowest buckling temperature is 3627°C and the associated mode is (25,1), the first integer in the bracket represents the circumferential mode and the second is the axial mode number.

As in the case of hemispherical shells B1 and C1 the buckling temperature increase with increase in the initial number of harmonics and immediately decrease and reach a low value and the buckling temperature is 2436°C for mode (8,1) and 1857°C for mode (10,1). Beyond mode (8,1) and (10,1) the buckling temperature increases slowly with increase in the number of harmonics. Considering the three shell configurations it is seen from Fig. 5 that for circumferential modes beyond 20 it is seen that the buckling temperature does not increase greatly as the mode number increases.

A study on the distribution of the stress resultants and moment resultants will be dealt subsequently in order to understand how each of these quantities, stress resultants and moment resultants, effect the buckling temperature and which among these quantities is more crucial in influencing the buckling temperature. Fig. 6 (a) and (b) shows the distribution of the meridional stress resultants, N_{ss}, and circumferential (or hoop) stress resultants, $N_{\theta\theta}$, along the meridian of the hemispherical shell with the circular edges clamped.

The axial stress resultants, N_{ss}, in general are very large over a small meridional length from the circular cut-out edge. The stress resultants are compressive for shell A1 and tensile for shell B1 and C1. As we move from the cut-out region towards the larger circular edge, the stress resultants

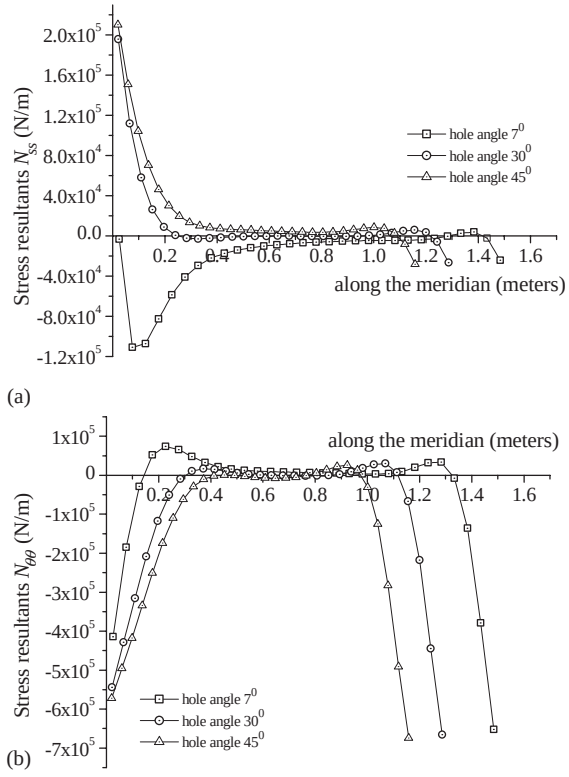

Fig. 6. (a, b) Distribution of meridional and hoop stress resultants for hemispherical shell with $a/h = 100$, clamped–clamped boundary condition.

are very small in magnitude and again over a small length near to the larger circular edge the stress resultants increase marginally and are compressive in nature. Looking into the distribution of hoop stress resultants $N_{\theta\theta}$, Fig. 6(b), it appears to be more or less symmetric about the middle of the meridian. It is noted that the stress resultants are highly compressive near the clamped circular edges and spread over a small definite length from the clamped edges and over the midportion of the shell the hoop stress resultants, $N_{\theta\theta}$, are negligible in magnitude similar to N_{ss}. For shell A1 the stress resultants N_{ss} and $N_{\theta\theta}$ are compressive but the magnitude of $N_{\theta\theta}$ is large compared to N_{ss}. For shells B1 and C1, the axial stress resultant, N_{ss}, are tensile but $N_{\theta\theta}$ is compressive. One needs to take very close look at the compressive nature of the circumferential stress resultants $N_{\theta\theta}$ distribution, which vary depending on the cut-out size at the apex of the shell. Accordingly from Fig. 6 (b), we observe that for shell A1 the distribution of $N_{\theta\theta}$ occurs for a small length compared to shells B1 and C1. Thus it is evident that the magnitude of buckling temperature is mostly governed by the stress resultants in the circumferential direction rather than the quantity N_{ss}. In the studies presented by Ganesan and Kadoli [29] on the thermal buckling of cylindrical shells, it was found that the buckling temperatures were mostly governed by meridional stress resultants, N_{ss}. Thus we see a change in the physical quantity from N_{ss} to $N_{\theta\theta}$, which produces the most influence on the buckling temperature. This can be attributed to the change in the geometry, i.e. spherical shells have double curvature when compared to cylindrical shell. The circumferential stress resultants are high in magnitude and compressive for shells B1 and C1 when compared to shell A1. Hence the buckling temperatures are comparatively lower in case of shells B1 and C1 when compared to shell A1.

The distribution of the moment resultants, M_{ss} and $M_{\theta\theta}$ are also presented in Fig. 7(a) and (b). The magnitudes of the moment resultants are very small when compared to the stress resultants.

Similar numerical studies are carried out on a hemispherical shell with $a/h = 500$ and keeping the rest of the geometrical parameters the same. This shell is much thinner, 2.0 mm, compared to the previous shell, 10.0 mm. The lowest buckling temperature associated with first 40 modes is presented in Fig. 8. For this shell the buckling temperatures are very low when compared to the shell with $a/h = 100$. This is expected since the thickness of the shell is less.

The trend in buckling temperature are similar to that observed for shell with $a/h = 100$. The important difference observed is that the maximum among the first axial mode buckling temperature will differ in the mode number. For example, peak buckling temperature for shell B1 with $a/h = 100$ is mode (2,1) whereas for shell B2 with $a/h = 500$ it is (5,1). Thus with larger a/h the maximum among the lowest buckling temperature shifts to higher modes. It is also found that the buckling temperatures are much lower for higher circumferential modes especially for shell with cut-out angles 30° and 45°, as low as 350°C. Referring to Fig. 8, the lowest buckling temperature for shell A2 is 1178°C, for B2 is 304.8°C and for C2 is 241°C. The corresponding mode numbers are (5,1), (14,1) and (19,1), respectively. Further the stress resultants and moment resultants are examined in order to ascertain which among these have a dominating influence on the buckling temperature. Fig. 9(a) and (b) shows the variations of the stress resultants, N_{ss} and $N_{\theta\theta}$, for shell with $a/h = 500$ and clamped–clamped boundary condition.

The distribution of the stress resultants is more or less similar to that observed in the case of shells with $a/h = 100$ in Fig. 6(a) and (b), but the magnitudes are high. The circumferential stress resultants are very much high and compressive in nature when compared to the stress resultants N_{ss} which are tensile in nature. Since buckling mainly occurs due to increase in the compressive

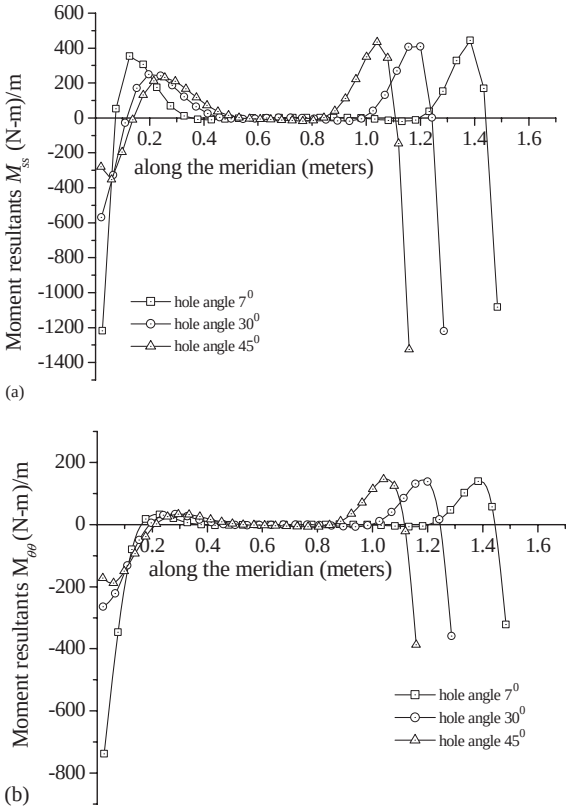

Fig. 7. Distribution of moment resultants for hemispherical shell with $a/h = 100$ and clamped–clamped boundary condition.

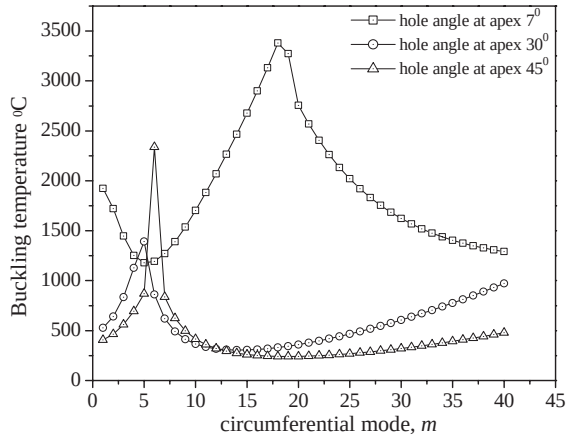

Fig. 8. Lowest buckling temperatures for hemispherical shell with $a/h = 500$ and clamped–clamped boundary condition.

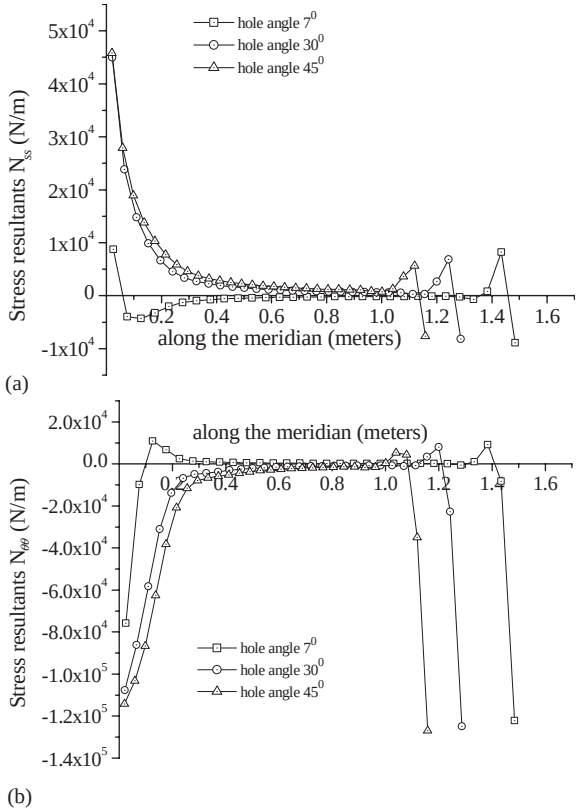

Fig. 9. (a,b) Distribution of meridional and hoop stress resultants for hemispherical shell with $a/h = 500$ and clamped–clamped boundary condition.

loading, it is clear that the circumferential stress resultants in the case of the hemispherical shells play a major role in dictating the thermal buckling temperature. The circumferential stress resultants, $N_{\theta\theta}$, are higher in magnitude for the shell C2 and decrease for shell B2 and A2 in that order. Hence the shell with cut-out angle of 45° has the lowest magnitude of thermal buckling temperature whereas the shell A2 with cut-out angle 7° has the highest buckling temperature. The moment resultants have least role to dictate the buckling temperature, and in fact these quantities are comparatively very small in magnitude and the variations of the same along the meridian are not presented here.

From the above study presented it is clear that in general the buckling temperatures are high in magnitude for hemispherical shells with clamped–clamped boundary condition. Shells with high a/h ratio will have lower buckling temperature. Among the shells considered in the study, the larger cut-out angle will tend to reduce the buckling temperature enormously.

3.4. Thermal buckling temperature for a hemispherical shell with clamped–free boundary condition

Fig. 2(c) illustrates typical hemispherical shell with cut-out at apex and clamped at the larger circular edge and the smaller circular edge at the apex is free from constraints. Numerical studies

on the thermal buckling temperature and distribution of stress and moment resultants are carried out on hemispherical shells with $a/h = 100$ and 500. The angle subtended by the cut-out with respect to the center of shell is 7°, 30° and 45°. Figs. 10 and 11 illustrates graphically the lowest thermal buckling temperature for the shells with $a/h = 100$ and 500. It is evident from the figures that the buckling temperatures are excessively large.

Referring to Fig. 10, it is noticed that the buckling temperatures are of the order of hundred thousand for the first circumferential mode irrespective of the size of the cut-out angle at apex. Smaller the cut-out size larger the temperature and it reduces with increase in cut-out size. For modes beyond ten the buckling temperatures reduce to the order of thousands and further as the number of circumferential harmonic increase the temperature reduces continuously to a low buckling temperature and beyond mode (26,1) the buckling temperature increases. The minimum among the lowest buckling temperatures are 3618.4°C, 3392.6°C and 3198.7°C, respectively, for

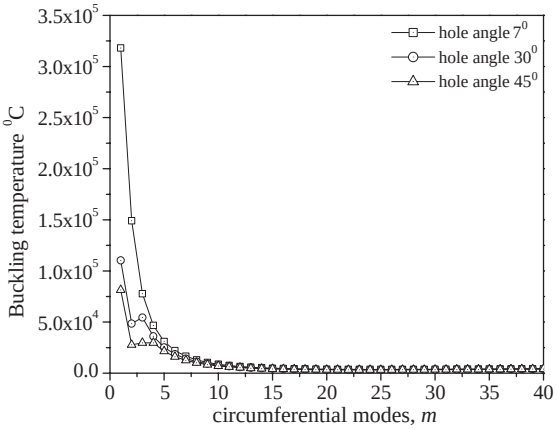

Fig. 10. Lowest thermal buckling temperature for hemispherical shell with $a/h = 100$ and clamped–free boundary condition.

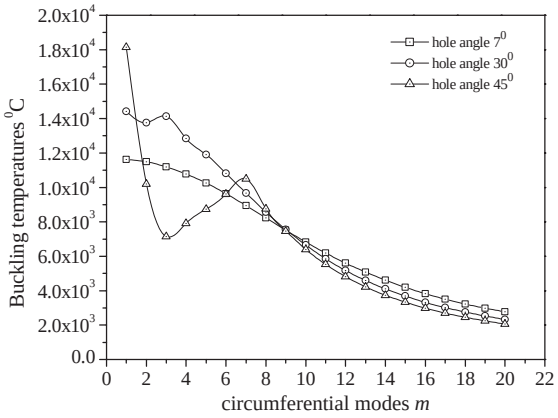

Fig. 11. Lowest buckling temperature for clamped–free hemispherical shell with $a/h = 500$.

shell A1, B1 and C1. The corresponding modes are (25,1), (24,1) and (24,1). Fig. 11 likewise illustrates the lowest buckling temperature associated with first 20 circumferential modes for a shell with $a/h = 500$. The buckling temperatures when compared to the shell with $a/h = 100$ are lower and of the order of ten thousands for the first few lower modes and beyond the mode number (8,1), the buckling temperatures are of the order of thousand. When compared to shell with $a/h = 100$, we do notice a distinct trend that, larger cut-out size at the apex will lead to lower buckling temperature. In case of this shell with $a/h = 500$, which means smaller shell thickness, we notice from Fig. 11 that (i) for the first mode buckling temperature is high for shell C2 and low for shell A2. Shell B2 has temperature intermediate to the above two. (ii) For the next few modes, i.e. from mode number (2,1)–(5,1) the buckling temperature for shell C2 are lower when compared to shell A2 and shell B2. (iii) For modes (7,1) and (8,1) the trend is same as described in point (i). Finally, (iv) beyond mode (9,1) the temperature reduces, with shell C2 having the lower temperatures and shell A2 having higher temperatures. The minimum among the lowest buckling temperature for shell A2, B2 and C2, respectively, are 1227°C, 985° and 855°C and the associated modes are (49,1), (49,1) and (48,1). It should be pointed out here that for a clamped–free shell, the lowest buckling temperatures are associated with very large number of circumferential waves.

Fig. 12(a) and (b) shows the distribution of N_{ss} and $N_{\theta\theta}$ along the meridian of the shell and are plotted from the free end (i.e. cut-out at apex) of the shell to the clamped circular edge, for shell with $a/h = 100$. It is observed that N_{ss} is smaller in magnitude and compressive over a small length from the free edge of the shell, as we move inwards the stress resultant N_{ss} will take on a negligible value. Further moving towards the larger circular edge, N_{ss} increases and is tensile in nature and moving closer to the edge, it changes sign and become excessively compressive. The stress resultants for shell C1 is high and compressive when compared to shell B1 and A1, especially over the region at the larger circular edge of the shell (i.e. near the clamped edge of the shell).

A look into Fig. 12(b) showing the distribution of the circumferential stress resultants $N_{\theta\theta}$, reveals that it is more or less close to zero as one starts moving from the cut-out edge towards the larger circular edge. As one moves towards the larger circular edge the circumferential stress resultants increase and are tensile over a small meridional length and further it changes sign and steeply increase to a maximum value (compressive sense). This nature of distribution is true for all the three shells. Apart from this it also seen that the maximum magnitude of $N_{\theta\theta}$ is developed in shell C1. However, the difference in maximum magnitude of $N_{\theta\theta}$ among the three shells is not very large. Thus it can be inferred that the maximum magnitude (and compressive nature) of N_{ss} as well as $N_{\theta\theta}$ very close to the fixed edge of the shell should be the main reason for the low magnitude of thermal buckling temperature for shell C1 (i.e. shell with cut-out subtending angle 45° at the center of the shell) when compared to shell B1 and A1.

Fig. 13(a) and (b) shows the distribution of the moment resultants M_{ss} and $M_{\theta\theta}$ for a clamped–free shell with $a/h = 100$. The distribution pattern is similar to that of N_{ss} or $N_{\theta\theta}$. The difference is that close to the cut-out circular edge M_{ss} are tensile and $M_{\theta\theta}$ is compressive and lower in magnitude. The magnitude of moment resultants are very small compared to the stress resultants. The influence of the moment resultants on the magnitude of buckling temperature may not be as serious as that due to stress resultants.

The distribution of the stress resultants for a clamped–free shell with $a/h = 500$ are presented in Fig. 14(a) and (b). The distribution of the stress resultants even though is similar to that seen in

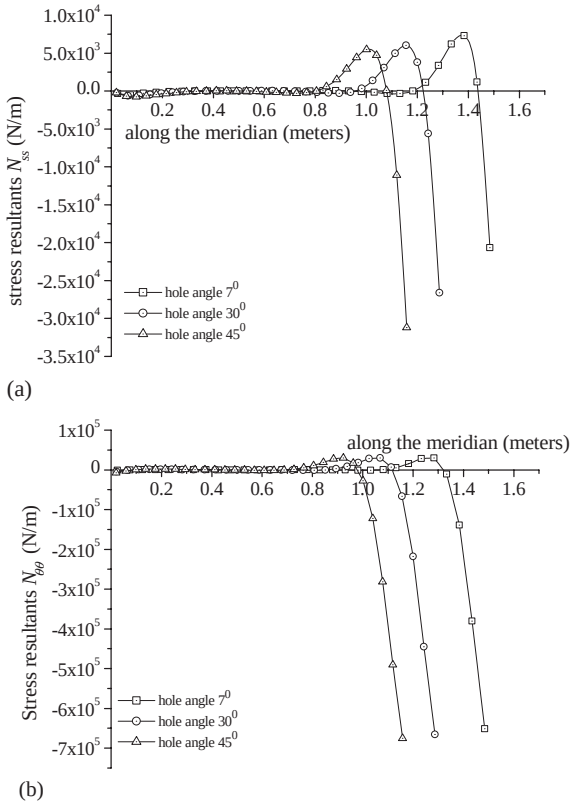

Fig. 12. (a, b) Distribution of stress resultants for hemispherical shell with $a/h = 100$ and clamped–free boundary condition.

Fig. 12(a) and (b), there are subtle differences that needs to be pointed. The stress resultants N_{ss} are high over a small region near about the clamped edge. The sign of the stress resultants change abruptly within this small region of the shell. The stress resultants remain more or less negligible for the rest of the region of the shell. The only difference one notices is that the negative maximum of N_{ss} is almost same for the three shells (namely shell A2, B2 and C2), which is not so in case of shell with $a/h = 100$. When one compares the stress resultant $N_{\theta\theta}$ (Figs. 12(b) and 14(b)) there isn't but difference in the distribution pattern. The moment resultants, M_{ss} and $M_{\theta\theta}$ are very less compared to N_{ss} and $N_{\theta\theta}$. It is clear on comparison of Fig. 14(b) with Fig. 14(a), that the magnitude of $N_{\theta\theta}$ is much greater when compared to N_{ss}. This gives a clear indication about the role of $N_{\theta\theta}$ influencing the magnitude of buckling temperature. Thus for a clamped–free shell C2 the buckling temperature are much lower compared to shell B2 and A2, see Fig. 11. It is probably felt that the very high buckling temperatures for various modes obtained by the present analysis for the shell with the larger circular edge clamped and edge formed by cut-out left free can be attributed to the fact that the static stiffness of the shell must be very large. This large static stiffness under specified boundary condition must have nullified the effect of initial stress resultants.

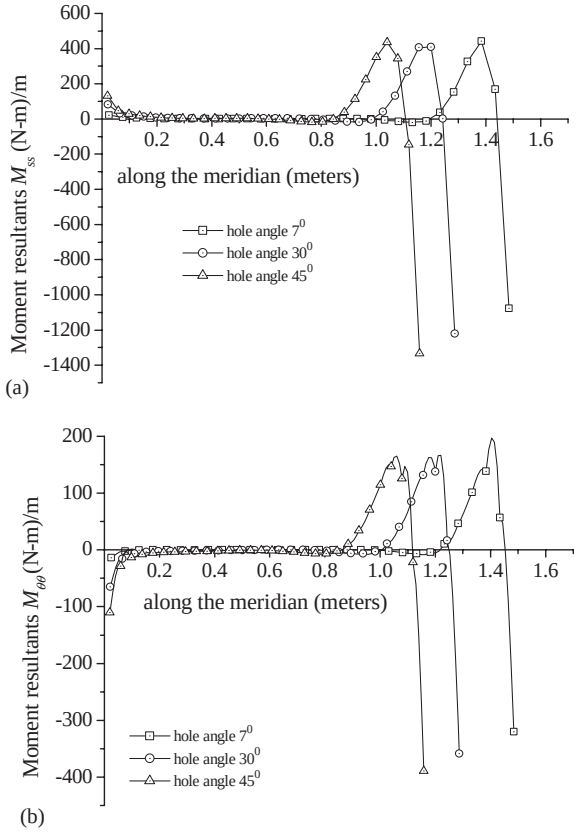

Fig. 13. (a, b) Distribution of the moment resultants in hemispherical shell with $a/h = 100$ and clamped–free boundary condition.

3.5. *Free vibration characteristics of hemispherical shells with cut-out subjected to steady state axisymmetric temperature*

In this section we present the effect of temperature on the free vibration natural frequency of the hemispherical shell with different cut-out angle. The geometric stiffness matrix also contributes to the stiffness of the shell. It is already seen in the earlier section that the thermal buckling temperatures are very high especially in case of clamped–free hemispherical shell. The same is true in case of the hemispherical shell with $a/h = 100$ for clamped–clamped edges. But it is found in case of hemispherical shell with $a/h = 500$ and clamped edges that the lowest thermal buckling temperature for various circumferential harmonics are quite high. Hence from this practical point of view, the temperatures do permit to present numerical results on free vibration beyond certain temperature. Few typical results have been presented for modes (10,1), (15,1) and (18,1). The lowest thermal buckling temperatures for these modes are listed in Table 4. The maximum temperature considered for analysis is restricted to a much lower temperature mainly from the point of view of practical aspects like materials at high temperature becoming soft and

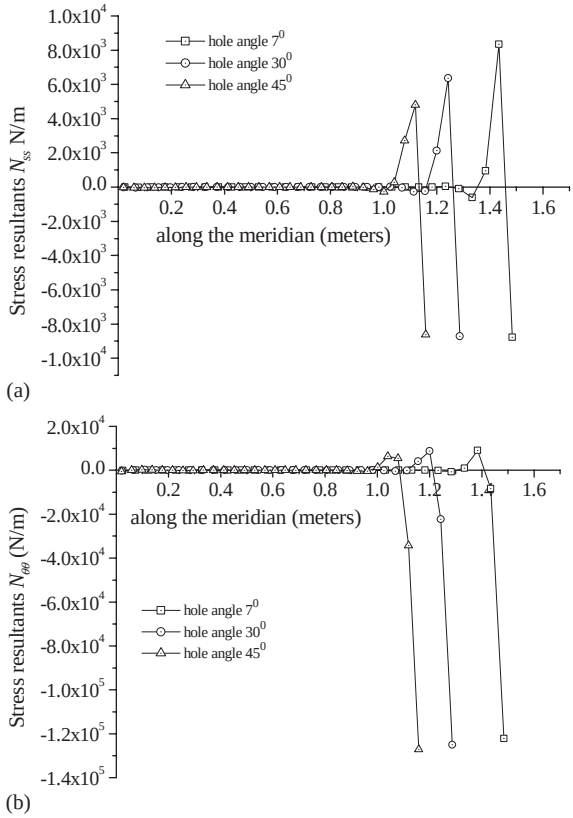

Fig. 14. (a, b) Distribution of stress resultants in a clamped–free hemispherical shell with $a/h = 500$.

Table 4
Buckling temperatures of selected modes of a hemispherical shell with $a/h = 500$ and clamped edges

Sl. No.	Mode	Cut-out angle at apex		
		7°	30°	45°
1	(10,1)	1703.6	366.0	416.2
2	(15,1)	2678.2	306.0	260.9
3	(18,1)	3378.7	330.9	242.0

continuous operation at high temperature should be avoided. Further at high temperature the elastic limit of the material decreases more rapidly than the elastic modulus. The maximum temperature used in the analysis is listed in Table 5.

Fig. 15–17 illustrates the effect of temperature on the first axial mode free vibration natural frequency of the shells. Shell with cut-out angle 7° has high buckling temperature. The frequencies do not reduce appreciably with increase in temperature.

This can probably be attributed to high static stiffness of the shell. For shells with larger cut-out angle, 30° and 45°, the behavior of the natural frequencies with increasing temperature is as

Table 5
Maximum temperature considered for free vibration analysis

Sl. No.	Mode	Cut-out angle at apex		
		7°	30°	45°
3	(10,1)	370.4	328.7	356.6
4	(15,1)	345.5	271.7	228.6
5	(18,1)	369.4	314.4	242.0

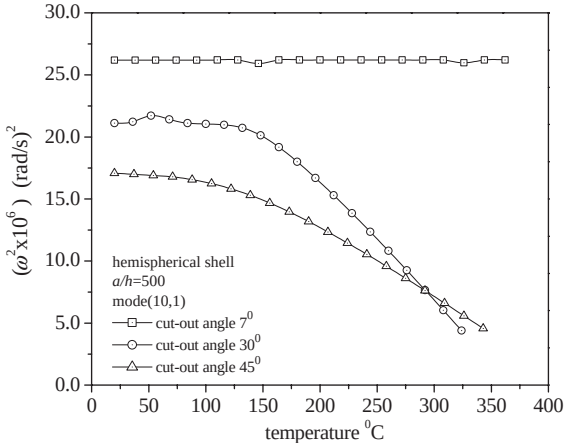

Fig. 15. Effect of temperature on the natural frequency of hemispherical shell with clamped–clamped edges for mode (10,1).

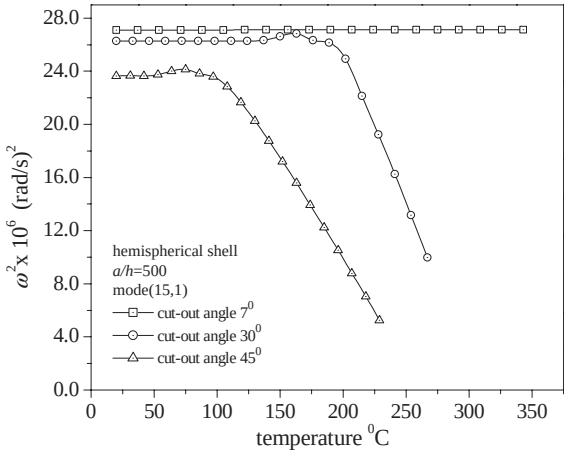

Fig. 16. Effect of temperature on the natural frequency of hemispherical shell with clamped–clamped edges for mode (15,1).

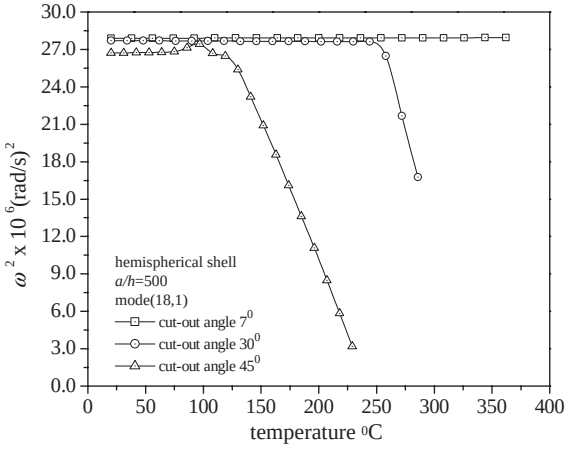

Fig. 17. Effect of temperature on the natural frequency of hemispherical shell with clamped–clamped edge for mode (18,1).

expected. The natural frequencies decrease very slowly with the initial increase in temperature, for temperatures close to the buckling temperature the natural frequencies decrease drastically and become zero at the buckling temperature.

It is quite reasonable to mention that the stress resultants increase as the temperature increases, hence the overall stiffness of the shell reduces. Fig. 18(a) and (b) illustrates the distribution of the stress resultants N_{ss} and $N_{\theta\theta}$ in a shell with cut-out angle 30°, $a/h = 500$ and clamped edges for three temperature cases. The circumferential stress resultant, $N_{\theta\theta}$, is predominantly high and concentrated near the clamped circular edges. Whereas, the meridional stress resultants, N_{ss}, is high near the cut-out at the apex when compared to the larger circular edge. Apart from this, the magnitude of N_{ss} is less compared to $N_{\theta\theta}$.

4. Conclusions

Linear static thermal buckling and free vibration analysis of hemispherical shells with cut-out at apex is presented. The hemispherical shell is geometrically perfect and is subjected to a uniform temperature rise. FSDT describes the kinematic relations for the general shells of revolution. The field variables are expressed using Fourier series in the circumferential direction and the semi-analytical method is used to construct the finite element matrices. The finite element formulation for linear static thermal buckling analysis was verified with the results reported in literature. Detailed parameter studies are carried out on hemispherical shells with $a/h = 100$ and 500 (or $h/a = 0.01$ and 0.002), cut-out angle of 7°, 30° and 45°, and for two edge conditions (namely clamped–clamped and clamped–free). The distribution of meridional and hoop stress resultants were plotted to obtain an insight into their influence on the magnitude of thermal buckling temperature. The effect of cut-out angle and boundary conditions on the magnitude of thermal buckling temperature and free vibratory natural frequency of heated hemispherical shell were clearly examined. The following are the inferences obtained from the study:

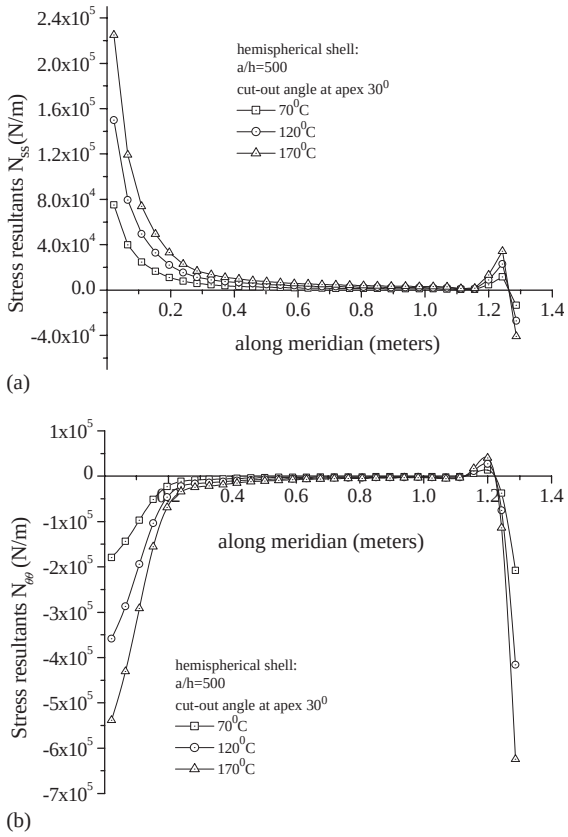

Fig. 18. Distribution of stress resultants in hemispherical shell for three temperature cases. a/h 500, clamped–clamped boundary condition and cut-out angle 30°.

1. The lowest thermal buckling temperatures are largest for hemispherical shell with $a/h = 100$ compared to $a/h = 500$. Hence thickness of the shell greatly influences the buckling temperature.
2. The magnitude of the lowest thermal buckling temperatures for various circumferential modes is excessively high for hemispherical shell with clamped–free boundary condition when compared to clamped–clamped shell. The associated circumferential mode number is also very high.
3. For hemispherical shell with clamped–clamped boundary condition, irrespective of the a/h ratio, the lowest buckling temperature for shells with larger cut-out will be lower when compared to shell with smaller cut-out.
4. For Clamped–clamped hemispherical shells with larger cut-out size (i.e. 30° and 45°), the trend in the magnitude of lowest thermal buckling temperature for various circumferential modes are more or less similar irrespective of a/h ratio. The influence of a/h is felt only in the associated circumferential mode number for higher of the lowest thermal buckling temperature. The mode

number increases as the a/h ratio increases. Similar characteristic feature is observed in case of hemispherical shell with clamped–clamped edge and smaller cut-out size at apex (i.e. 7°).

5. It is found that primarily the hoop stress resultant dictates the magnitude of the thermal buckling temperature, either in the case of the clamped–clamped or clamped–free hemispherical shells.
6. The thermal buckling temperatures for various modes are excessively high for shells with a/h 100 for clamped–clamped and clamped–free edge conditions and for clamped–free shell with a/h 500, indicating that the static stiffness of these shells are high. Hence the effect of initial increase in temperature (say up to 330°C) on the variation of natural frequency is not felt much. This can be easily inferred from the studies carried out on a clamped–clamped shell with $a/h = 500$ and smaller cut-out at apex, i.e. 7°, which also has high buckling temperature. For the same shell with $a/h = 500$ and larger cut-out at apex, the lowest thermal buckling temperatures are comparatively lower for higher circumferential modes. Hence the effect of temperature on the free vibration natural frequency is felt clearly, the frequency gradually decreases as the temperature of the shell increases.

Acknowledgements

The untiring efforts devoted by the anonymous reviewers for this article is highly acknowledged. The authors are grateful to the reviewers for their useful suggestions on this article.

References

[1] J.G. Teng, Buckling of thin shells: recent advances and trends, *Applied Mechanics Review* 49 (12) (1996) 263–274.
[2] E.A. Thornton, Thermal buckling of plates and shells, *Applied Mechanics Review* 46 (10) (1993) 485–506.
[3] M.S. Qatu, Recent research advances in the dynamic behavior of shells: 1989–2000, Part 2: homogeneous shells, *Applied Mechanics Review* 55 (5) (2002) 415–433.
[4] N. Noda, Thermal stresses in materials with temperature-dependent properties, *Applied Mechanics Review* 44 (9) (1991) 383–397.
[5] A.K. Noor, W.S. Burton, Computational models for high-temperature multilayered composite plates and shells, *Applied Mechanics Review* 45 (10) (1992) 419–445.
[6] K.M. Liew, C.W. Lim, S. Kitipornchai, Vibration of shallow shells: a review with bibliography, *Applied Mechanics Review* 50 (8) (1997) 431–444.
[7] R.R. Archer, On the influence of uniform stress states on the natural frequencies of spherical shells, *Transactions of the American Society of Mechanical Engineers, Journal of Applied Mechanics* 29 (1962) 502–505.
[8] J.R. Fitch, The buckling and post-buckling behavior of spherical caps under concentrated load, *International Journal of Solids and Structures* 4 (1968) 421–446.
[9] P.T. Pedersen, J.J. Jensen, Buckling behavior of imperfect spherical shells subjected to different load conditions, *Thin-Walled Structures* 23 (1995) 41–55.
[10] J.C. Yao, Buckling of a truncated hemisphere under axial tension, *American Institute of Aeronautics and Astronautics Journal* 1 (10) (1963) 2316–2319.
[11] M.A. Krenzke, T.J. Kiernan, Elastic stability of near-perfect shallow spherical shells, *American Institute of Aeronautics and Astronautics Journal* 1 (12) (1963) 2855–2857.
[12] N.C. Huang, Unsymmetrical buckling of thin shallow spherical shells, *Journal of Applied Mechanics* 31 (1964) 447–457.

[13] J.R. Fitch, B. Budiansky, Buckling and postbuckling behavior of spherical caps under axisymmetric load, *American Institute of Aeronautics and Astronautics Journal* 8 (4) (1970) 686–693.
[14] S. Gu, Buckling behavior of ring loaded shallow spherical shells with a center hole, *International Journal of Non-Linear Mechanics* 26 (2) (1991) 263–274.
[15] P.B. Gonçalves, Axisymmetric vibrations of imperfect shallow spherical caps under pressure loading, *Journal of Sound and Vibration* 174 (2) (1994) 249–260.
[16] H.E. Williams, Axisymmetric thermal stress in a thin spherical shell by the method of matched asymptotic expansions, *International Journal of Solids and Structures* 13 (1977) 747–769.
[17] G. Krizhevsky, Y. Stavsky, Refined theory for non-linear buckling of heated composite shallow spherical shells, *Computers and Structures* 55 (6) (1995) 1007–1014.
[18] B.D. Aggarwala, Thermal stability of bimetallic shallow spherical shells, *International Journal of Non-Linear Mechanics* 5 (1970) 49–62.
[19] R.H. Liu, Non-linear thermal stability of bimetallic shallow shells of revolution, *International Journal of Non-Linear Mechanics* 18 (5) (1983) 429–459.
[20] J. Jayaraman, K.P. Rao, Thermal stresses in a spherical shell with a conical nozzle, *Nuclear Engineering and Design* 48 (1978) 367–375.
[21] P. Jianping, I.E. Harik, Thermal stresses in spherical shells, *Journal of Aerospace Engineering* 6 (1) (1993) 106–110.
[22] R.K. Kapania, P. Mohan, Static, free vibration and thermal analysis of composite plates and shells using a flat triangular shell element, *Computational Mechanics* 17 (1996) 343–357.
[23] N.J. Hoff, Buckling at high temperature, *Journal of the Royal Aeronautical Society* 61 (1957) 756–774.
[24] D. Abir, S.V. Nardo, Thermal buckling of circular cylindrical shells under circumferential temperature gradients, *Journal of the Aerospace Sciences* 26 (1959) 803–808.
[25] W. Zuk, Thermal buckling of clamped cylindrical shells, *Journal of the Aerospace Sciences* 25 (1957) 389.
[26] S.K. Radhamohan, J. Venkataramana, Thermal buckling of orthotropic cylindrical shells, *American Institute of Aeronautics and Astronautics Journal* 13 (3) (1975) 397–399.
[27] S.Y. Lu, L.K. Chang, Thermal buckling of conical shells, *American Institute of Aeronautics and Astronautics Journal* 5 (10) (1967) 1877–1882.
[28] M.R. Eslami, H.R. Ghorbani, M. Shakeri, Thermoelastic buckling of thin spherical shells, *Journal of Thermal Stresses* 24 (2001) 1177–1198.
[29] N. Ganesan, R. Kadoli, Buckling and dynamic analysis of piezothermoelastic composite cylindrical shell, *Composite Structures* 59 (1) (2003) 45–60.
[30] S. Ramalingeswara Rao, N. Ganesan, Interlaminar stresses in shells of revolution, *Mechanics of Composite Materials and Structures* 3 (1996) 321–339.
[31] S. Ramalingeswara Rao, Static and Dynamics Problems in Laminated Beams and Axisymmetric Shells, Ph.D. Thesis, Indian Institute of Technology Madras, Chennai, India, 1997.